Numerical analysis of cyclorotor aerodynamic properties in hovering state

To cite this article: Shawn Cogan and Louis Gagnon 2022 *IOP Conf. Ser.: Mater. Sci. Eng.* **1226** 012039

Numerical analysis of cyclorotor aerodynamic properties in hovering state

Shawn Cogan[1] and Louis Gagnon[2]

[1] Master Student, University of Stuttgart, Germany
[2] Postdoctoral Fellow, Institute of Aerodynamics and Gas Dynamics, University of Stuttgart, Germany

E-mail: coganpshawn@gmail.com

Abstract. Cyclorotors employ cyclically pitched axial rotor blades to create an extremely maneuverable propulsion system. The pitch angle throughout one rotation is defined so that the resulting blade angle of attack follows a prescribed function that generates lift. The lift and drag produced is also affected by curvilinear flow, dynamic stall, and induced velocities, all of which affect the resulting angle of attack. These factors form complex relationships that are difficult to model analytically, making it hard to predict a cyclorotor's performance. Here, a numerical model is presented which can be used to predict thrust and power draw of different cyclorotor configurations. Parameters include airfoil, number of rotor blades, rotational velocity, pivot function, fluid properties and Reynold's number. The numerical model builds on previously implemented approximations but focuses on time-efficient calculations so that many configurations may be calculated in an iterative process. In each iteration the parameters can be adjusted according to machine learning or other metaheuristic optimization algorithms to determine an optimal configuration.

1. Introduction

A cyclorotor (cyclogyro, cyclocopter, cycloidal propeller) is a heavier-than-air flight vehicle capable of vertical takeoff and landing using cyclically pitched, horizontal rotor blades. Typical configurations consist of 4 to 6 rotor blades per rotor, which spin parallel to each other around a central axis. As they turn, the rotor blades pivot around their longitudinal axis. The pivot function is periodic, with each rotation about the common axis defining the frequency of the pitching function. Pivot functions resemble a sine curve and function to generate a constant lift, keeping a positive angle of attack in quadrants one and two, and a negative angle of attack in quadrants 3 and 4. However, the pivot functions can be adapted to be more efficient in different flight envelopes, for example during hovering, forward flight, or maneuvering. A key characteristic of a cyclorotor is that it can very rapidly change its pivot function, almost instantly changing direction and magnitude of thrust. Magnitude of thrust is altered by changing the amplitude of the pivot function, and the direction of thrust is changed by shifting the phase of the pivot function.

2. Methods

The goal of the work is to create a model to give a good overview of the performance of a cyclorotor, trading accuracy for computational speed. It models thrust and power draw for a

cyclorotor with almost any combination of radius, blade number, profile, rpm, chord length, and pivot function. The model is tested with six blades, each using a NACA 0012 airfoil. A symmetrical airfoil is chosen because it must provide lift with both a positive and negative angle of attack. The following sections describe the development of the parametric model used to optimize the pivot function.

2.1. Parametric Model

The parametric model relies on several key theories and assumptions. Most important is an approximated incompressible steady flow over each profile without flow separation. The lift and drag of each profile therefore depend only on α and U_∞, and can be taken from experimental values [1, 2]. Polar diagrams that correspond to the Reynolds number and airfoil of the cyclorotor are approximated by polynomials, which are reasonably accurate at low angles of attack [3]. Lift is approximated with a series of 2^{nd} and 3^{rd} order polynomials and drag with 2^{nd} order polynomials. Different polynomials are used to approximate the polar curve before and after the critical angle of attack. Due to the symmetrical airfoil, the lift polar diagram is an odd function and the drag polar diagram an even function. Rectilinear flow is also assumed, which presumes a parallel inflow of air over each profile. For this to hold true, angular velocity and acceleration must be negligible. Other factors such as gravity, structural influence and ground effect are also assumed to be negligible. If these assumptions hold true, the lift and drag of each profile can be evaluated at each time step, averaged over one rotation and the thrust and power consumption of the cyclorotor evaluated. What cannot be ignored is the induced velocity, or downwash which the cyclorotor creates, as it greatly affects the aerodynamic angle of attack of each profile. This effect can function to reduce even relatively high pitching angles.

Streamtube (STT) and double-multiple streamtube theories (D-MSTT) [4, 5, 6] are used to approximate the induced velocity. The downwash is assumed to run through a tube of air, only entering and exiting at the ends of the stream tube. Actuator disk theory and Bernoulli's continuity equations are applied to a stream tube running through the cyclorotor, and an induced velocity, dependent on thrust produced, is calculated. The calculated velocity alters the aerodynamic angle of attack, which in turn changes the thrust, and a new velocity through the stream tube is calculated. In this way, the induced velocity is iteratively determined for each stream tube. In the STT one stream tube is used for the whole cyclorotor, and in the D-MSTT several parallel stream tubes bisect the cyclorotor. The number of stream tubes varies and can be chosen based on computational capacity. The stream tubes always run parallel to the thrust vector of the cyclorotor.

On account of the aerodynamic values being extracted from polar diagrams, the parametric model solves for a periodic steady-state rotation.

2.2. Pivot Function

One of the first methods of regulating the pitching function of a cyclorotor was through the use of the four-bar mechanism. It is a simple mechanism that does not rely on a separate power source other than a servo controller, and can operate at high rotational velocities. Each rotor blade is connected to the center of the rotor by two bars which run radially from two points on the airfoil to two points in the center of the rotor. They are both hinged on both ends so that the cyclorotor can turn freely. One bar connects to the center of rotation of the cyclorotor, while the other one connects to a point slightly offset from the center of rotation. As the cyclorotor turns, this offset changes the angle of attack of the rotor blade and creates a periodic pivot function. The function can be derived through application of the law of sines and cosines. It is worth noting that the location of the pivot point (Figure 1, intersection of R and a) on the rotor blade does not affect the pitching function in the parametric model. Only the lengths of bars l and d (Figure 1) affect the pitch of the rotor. When accounting for angular acceleration,

the pivot point location affects the velocity and acceleration of the leading and trailing edge of each blade.

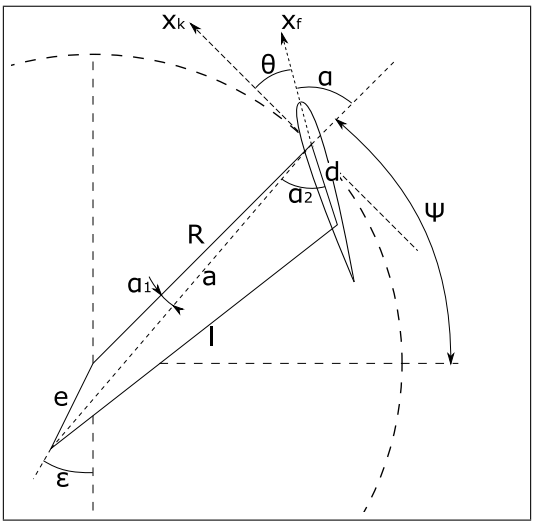

Figure 1. Variable definitions of a 4-bar mechanism.

However, as these values are assumed to have a minimal impact on performance the position of the pivot point has no impact in the simulation. It is usually set approximately 25% down the length of the chord from the leading edge.

Most of the variable definitions (Figure 1) are taken from [7] and [8], and have been used in several other parametric models. The pivot function is derived by comparing the two triangles that make up the four connected bars (e, l, d, R). From the law of cosines:

$$a = \sqrt{e^2 + R^2 - 2eR \cdot cos\left(\Psi + \varepsilon + \frac{\pi}{2}\right)} \tag{1}$$

and

$$\alpha_2 = arccos\left(\frac{a^2 + d^2 - l^2}{2ad}\right) \tag{2}$$

From the law of sines:

$$\alpha_1 = arcsin\left(\frac{e \cdot sin\left(\Psi + \varepsilon + \frac{\pi}{2}\right)}{a}\right) \tag{3}$$

The angle of attack can be written in terms of α_1 and α_2 as

$$\theta = \frac{\pi}{2} - \alpha_1 - \alpha_2 \tag{4}$$

resulting in the equation

$$\theta\left(\Psi\right) = \frac{\pi}{2} - arcsin\left(\frac{e \cdot cos\left(\Psi + \varepsilon\right)}{a}\right) - arccos\left(\frac{a^2 + d^2 - l^2}{2ad}\right) \tag{5}$$

As the cyclorotor rotates, α_1 will be contained in α_2 for

$$\frac{\pi}{2} - \varepsilon \leq \Psi \leq \frac{3\pi}{2} - \varepsilon \tag{6}$$

and equation 4 changes to $\theta = (\pi/2)+\alpha_1-\alpha_2$. However, $\Psi+\varepsilon+(\pi/2)$ is for this range between π and 2π, and according to equation 3, α_1 is negative. Together, the signs cancel out and equation 5 holds true for $0 < \Psi \leq 2\pi$. It is important to note that θ is negative when its local angle of attack is below the tangent line of the cyclorotor. Even though it may have a positive angle of attack in a global frame, its local angle of attack relative to its direction of movement can be negative.

2.3. Induced Velocity

As the cyclorotor produces thrust, it produces airflow antiparallel to the thrust vector. The flow of air changes the aerodynamic angle of attack on the rotor blades by several degrees. The induced velocity can be approximated with the actuator disk theory, assuming a constant induced velocity across an actuator disk.

In the single stream tube model (Figure 2), the induced velocity is assumed constant for every rotor blade at every position, and the actuator disk is a plane located in the center of the cyclorotor perpendicular to the thrust direction. The thrust produced is equal to

$$T = A \cdot (p_2 - p_1) \tag{7}$$

where p_1 is the pressure immediately above the actuator disk and p_2 the pressure immediately below. From the Bernoulli equation

$$p_2 - p_1 = \frac{1}{2}\rho \left(w_9^2 - w_0^2\right) \tag{8}$$

According to the actuator disk theory and Froude theory $w_1 = w_2$ and $w_1 - w_0 = w_9 - w_2 = \Delta w$ so that Equation 7 can be rewritten as

$$T = 2\rho A \left(w_0 + \Delta w\right) \Delta w \tag{9}$$

In hovering state $w_0 = 0$, the induced velocity can be written as

$$\Delta w \overset{\text{hov.}}{=} \sqrt{\frac{T}{2\rho A}} = \frac{1}{2}\sqrt{\frac{T}{\rho R s}} \tag{10}$$

where s is defined as the span of the cyclorotor. The induced velocity is determined iteratively as it is dependent on the thrust produced. To guarantee convergence of thrust and induced velocity, their values are inhibited by a dampening factor in each iteration

$$\begin{aligned} T_{new} &= T_{old} + (T_{calc} - T_{old}) \cdot \alpha_T \\ v_{i,new} &= v_{i,old} + (v_{i,calc} - v_{i,old}) \cdot \alpha_v \end{aligned} \tag{11}$$

The dampening factor value is chosen between 0 and 1, depending on the configuration. A high value leads to instability in the calculation and a low value increases the number of iterations required.

To yield more accurate results, the stream tube model can be expanded to the double-multiple streamtube model (Figure 3). The cyclorotor is divided up into several stream tubes, each of which has its own induced velocity. This way, a discretized velocity profile is solved across the diameter of the cyclorotor. For each time step, the induced velocity affecting a rotor is based on which stream tube the rotor is in at that time. Each stream tube is modeled by two actuator disks set up in tandem, meaning the outflow of the first actuator disk is equal to the inflow of the second actuator disk. The inflowing w_0 is accelerated radially to the upper induced velocity

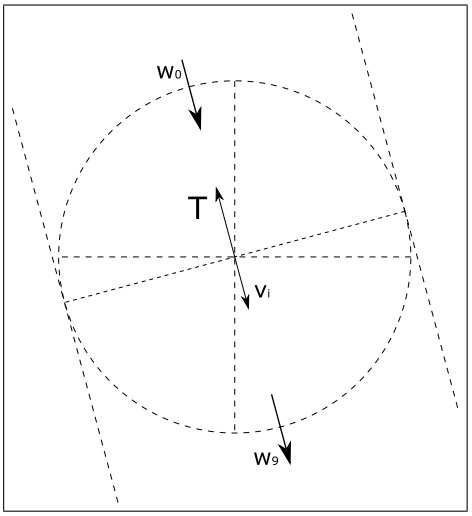

Figure 2. Single streamtube model.

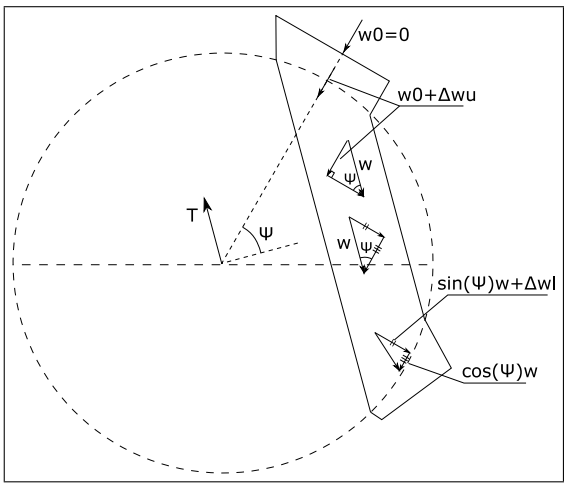

Figure 3. Stream tube in a double-multiple streamtube model.

$w_0 + \Delta w_u$. Once again applying Froude's theorem, the velocity far downstream behind the actuator disk will increase in speed by the same amount behind the actuator disk as it did in front. Thus, the velocity in the center of the cyclorotor is equal to $w_0 + 2 \cdot \Delta w_u$. However, the stream tube runs parallel to the thrust vector, and the induced velocity is bent by the stream of air in the other stream tubes. This increases the velocity in the center of the stream tube to

$$w = \frac{w_0 + 2\Delta w_u}{sin\left(\Psi\right)} \overset{\text{hov.}}{=} \frac{2\Delta w_u}{sin\left(\Psi\right)} \tag{12}$$

Applying equations 7 and 8,

$$T_u = \frac{1}{2}\rho A\left(w^2 - w_0^2\right) = \frac{1}{2}\rho A\left(\frac{w_0^2 + 4\Delta w_u w_0 + 4\Delta w_u^2}{sin\left(\Psi\right)^2} - w_0^2\right) \tag{13}$$

In hovering state, the induced velocity in the upper part of the stream tube is therefore

$$\Delta w_u \overset{\text{hov.}}{=} \sqrt{\frac{T_u sin\left(\Psi\right)^2}{2\rho A}} = \sqrt{\frac{T_u sin\left(\Psi\right)^2}{2\rho R d\Psi}} \tag{14}$$

The inflow velocity for the bottom actuator disk of the stream tube is no longer 0, but w (Equation 12). Equations 7 and 8 can also be rewritten as

$$T = \frac{1}{2}\rho A\left(w_9^2 - w_0^2\right) = \frac{1}{2}\rho A\left(w_9 + w_0\right)\left(w_9 - w_0\right) \tag{15}$$

and applying Froude's theorem

$$T = \frac{1}{2}\rho A\left(w_0 + 2\Delta w + w_0\right)\left(w_0 + 2\Delta w - w_0\right) = 2\rho A\left(w_0 + \Delta w\right)\left(\Delta w\right) \tag{16}$$

Applying equation 16 to the lower actuator disk,

$$T_l = 2\rho A\left(\vec{w} + \vec{\Delta w_l}\right)\left(\Delta w_l\right) \tag{17}$$

$$\begin{aligned} T_l &= 2\rho A \Delta w_l \sqrt{\left(w sin\left(\Psi\right) + \Delta w_l\right)^2 + \left(w cos\left(\Psi\right)\right)^2} \\ &= 2\rho A \Delta w_l \sqrt{w^2 + 2w\Delta w_l sin\left(\Psi\right) + \Delta w_l^2} \end{aligned} \tag{18}$$

Equation 18a is derived from the vector addition of w and Δw_l. Variable w is split into its counterparts in the direction of Δw_l (Figure 3). These were applied to cyclorotors by Yun *et al.* [9] and have been implemented in several other cyclorotor models, as well as wind turbine models [6, 4]. The induced velocities at the top and bottom of each stream tube, the thrust produced by the cyclorotor, as well as the direction of thrust of the cyclorotor are all interdependent, and must be solved iteratively.

3. Results

Below are the results of the parametric model, alongside values obtained from a 2D CFD simulation and from an experimental model. Both are tested at different configurations, with varying rotational velocity and pitching function. Differences between two-dimensional simulations and three-dimensional experiments are expected, due to the differences in flow and turbulence. Nonetheless, a close correlation between the approximated calculations and experimental values confirms that the model can distinguish and evaluate the performance of different configurations.

Experimental thrust and power consumption values for varying cyclorotor configurations were gathered by the Korea Aerospace Research Institute [9]. In order to measure only the aerodynamic effects of the blades, the weight of the scale and structure was subtracted from the thrust, and the power draw of the cyclorotor without the rotor blades was subtracted from the gross power draw. Both the maximum pitch angle as well as the rotational velocity are tested over a wide envelope to obtain a wide variety of results.

Significant losses in accuracy are noted at pitching functions 20° and 15° (Figure 5). This is explained by the coefficient of lift vs angle of attack curve, upon which the model depends to compute its thrust. As the critical angle of attack is reached, the thrust produced drops initially as flow separation occurs. However, as the angle of attack is increased further, the lift begins to increase again.

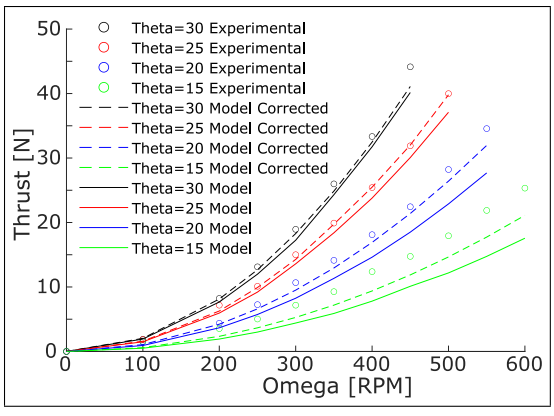

Figure 4. Thrust comparison of different pitching functions.

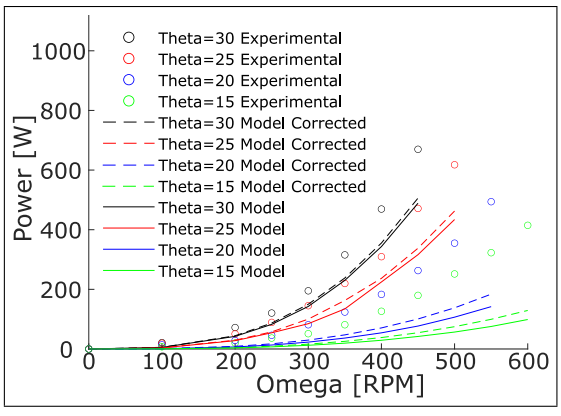

Figure 5. Power draw comparison of different pitching functions.

Additional simulations of the parametric model are run, in which the downwash in the center of the cyclorotor is slowed down by 5%. Equation 12 therefore becomes

$$w = 0.95 \cdot \frac{2\Delta w_u}{sin\,(\Psi)} \tag{19}$$

A similar method of correcting parametric results has been implemented by [10], where the correctional factor focuses on 2 and 3 dimensional differences. Further correctional factors could be applied, however, without concrete comparisons such as a prototype or 3D simulation it is not possible to fully justify these corrections.

It is assumed the downwash in the parametric model is faster than in the experimental results. Applying the correction factor of 0.95 to the downwash yields corrected results (Figures 4, 5).

CFD simulations allow for a more thorough comparison of thrust and power, as well as the flow of air inside the cyclorotor. Thrust is calculated by summing the integrated pressure and friction values over the surfaces of each airfoil. Similarly, the moment is calculated by integrating pressure and friction forces over the surface, as well as the distance of the cell from the center of the cyclorotor. The power draw is determined by multiplying the moment with the rotational velocity.

Comparing the thrust and power draw of several different CFD configurations (Figures 6 and 7), the thrust is as expected higher than the experimental values. With fewer disturbances and flow disruptions, the cyclorotor is able to displace more air in two dimensions than with a finite wing. Thrust and power draw follow a reliable trend between different rotational velocities.

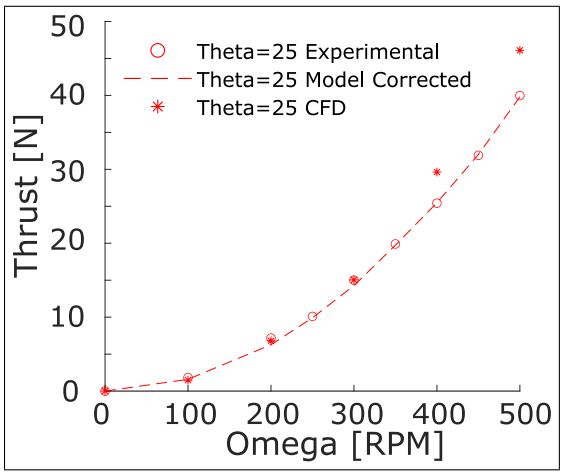

Figure 6. Thrust comparison with CFD simulations.

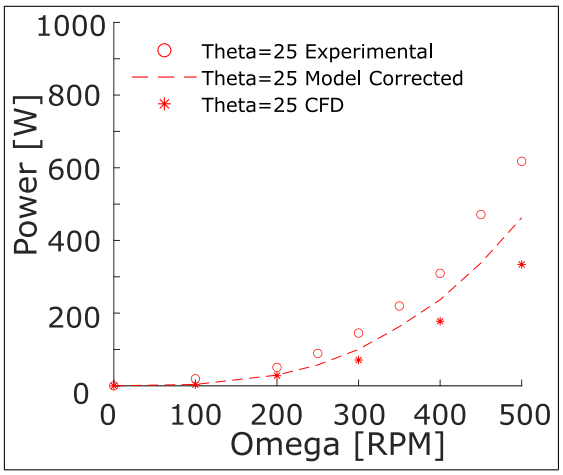

Figure 7. Power comparisons with CFD simulations.

4. Conclusions

Presented is a parametric numerical model capable of solving aerodynamic properties, relying on the Integral Momentum Theorem applied to actuator disks and stream tubes. A single stream tube model is used to model a cyclorotor for preliminary calculations and estimations. A variant of the single stream tube model, the double multiple stream tube model, is used for more accurate solutions. Velocities are calculated numerically in an iterative process, and determine thrust and power draw of different configurations.

To validate the results of the parametric model, a two-dimensional computational fluid dynamics simulation is run for each cyclorotor configuration and compared to the model. The parametric model is validated with experimental results as well. All three results exhibit similar values, though a 5% correctional factor is used to slow the induced velocity in the parametric

model. The largest deviation from expected values is seen in power draw, especially at low angles of attack and in the CFD simulation. However, differences in aerodynamic properties compare well between configurations, as long as configurations above or below critical angle of attack are compared.

Acknowledgments
The work of Louis Gagnon is supported by the Alexander von Humboldt foundation for the "A Novel and Simple Aircraft Requiring Minimal Power to Hover" project through their Research Fellowships for Postdoctoral Researchers.

References

[1] Sheldal R E and Klimas P C Aerodynamic characteristics of seven symmetrical airfoil sections through 180-degree angle of attack for use in aerodynamic analysis of vertical axis wind turbines Tech. rep. Sandia National Laboratories
[2] White F M 1998 *Fluid Mechanics* 4th ed (McGraw-Hill) ISBN 0070697167
[3] Singh K and Pascoa J 2019 *Journal of Fluids Engineering* **141**
[4] Strickland J H 1975 The darrieus turbine: A performance prediction model using multiple streamtubes Tech. rep. Sandia Laboratories Department of Mechanical Engineering, Texas Tech University, Lubbock, TX 79409
[5] Paraschivoiu I Double-multiple streamtube model for darrieus wind turbines Tech. rep. Institut de Recherche d'Hydro-Quebec
[6] Benedict M, Mattaboni M, Chopra I and Masarati P 2011 *AIAA* **49** 2430–43
[7] Higashi Y, Tanaka K, Emaru T and Wang H 2006 *IEEE/RSJ* 3261–66
[8] Leger J, Pascoa J and Xisto C 2015 *Journal of Aerospace Engineering* **229** 2163–77
[9] Yun C and Park I 2005 *American Helicopter Society* 24–35
[10] Benedict M 2010 *Fundamental Understanding of the Cycloidal-Rotor Concept for Micro Air Vehicle Applications* Ph.D. thesis University of Maryland